RSC Advances

PAPER

View Article Online
View Journal | View Issue

Cite this: *RSC Adv.*, 2024, **14**, 5764

Synergic effect of CaI_2 and LiI on ionic conductivity of solution-based synthesized $Li_7P_3S_{11}$ solid electrolyte†

Tran Anh Tu,[abc] Tran Viet Toan,[ab] Luu Tuan Anh,[ab] Le Van Thang[abc] and Nguyen Huu Huy Phuc *[abc]

Received 17th January 2024
Accepted 8th February 2024

DOI: 10.1039/d4ra00442f

rsc.li/rsc-advances

$Li_7P_3S_{11}$ doped with CaX_2 (X = Cl, Br, I) and LiI solid electrolytes were successfully prepared by liquid-phase synthesis using acetonitrile as the reaction medium. Their structure was investigated using XRD, Raman spectroscopy and SEM-EDS. The data obtained from complex impedance spectroscopy was analyzed to study the ionic conductivity and relaxation dynamics in the prepared samples. The XRD results suggested that a part of CaX_2 and LiI incorporated into the structure of $Li_7P_3S_{11}$, while the remaining part existed at the grain boundary of the $Li_7P_3S_{11}$ particle. The Raman peak positions of PS_4^{3-} and $P_2S_7^{4-}$ ions in samples $90Li_7P_3S_{11}$–$5CaI_2$ and $90Li_7P_3S_{11}$–$5CaI_2$–5LiI had shifted as compared to the $Li_7P_3S_{11}$ sample, showing that CaI_2 addition affected the vibration of PS_4^{3-} and $P_2S_7^{4-}$ ions. EDS results indicated that CaI_2 and LiI were well dispersed in the prepared powder sample. The ionic conductivity at 25 °C of sample $90Li_7P_3S_{11}$–$5CaI_2$–5LiI reached a very high value of 3.1 mS cm^{-1} due to the improvement of Li-ion movement at the grain boundary and structural improvement upon CaI_2 and LiI doping. This study encouraged the application of $Li_7P_3S_{11}$ in all-solid-state Li-ion batteries.

1. Introduction

Sulfide-based solid electrolytes (SE) have high potential for application in all-solid-state batteries because of their relatively high ionic conductivity and suitable mechanical properties compared with oxide-based and polymer-based SEs.[1,2] $Li_7P_3S_{11}$, $Li_{9.54}Si_{1.74}P_{1.44}S_{11.7}Cl_{0.3}$, $Li_{5.35}Ca_{0.1}PS_{4.5}Cl_{1.55}$ and $Li_{10.1}P_{2.95}Sb_{0.05}S_{12}I$ exhibited excellent ionic conductivities of about 17, 25, 10.2 and 5.9 mS cm^{-1} at 25 °C, respectively.[3–6] Among them, $Li_7P_3S_{11}$ has been thoroughly studied since it was invented.[7] $Li_7P_3S_{11}$ is usually prepared by solid-state reaction and achieves a highest ionic conductivity of about 17 mS cm^{-1} at 25 °C.[8] Researchers have studied the effects of many different substances such as Li_3PO_4, Li_3BO_3, Li_2ZrO_3 and P_2O_5 on the ionic conductivity of $Li_7P_3S_{11}$.[9–12] Murakami *et al.* studied $^{6/7}Li$ and ^{31}P solid-state NMR to investigate the origin of high ionic conductivity of $Li_7P_3S_{11}$ and found that the significant motion fluctuation of the P_2S_7 tetrahedral unit above 310 K facilitated the Li-ion movement, resulting in high ionic conductivity.[13] Seino *et al.* found that $Li_7P_3S_{11}$ glass ceramic with the crystallinity ranging from 50% to 80% reached its highest ionic conductivity.[14]

The liquid phase synthesis of $Li_7P_3S_{11}$ has been recently introduced and takes the advantage of electrode composite preparation.[15,16] Dimethoxy ethane was the first solvent ever used to prepared $Li_7P_3S_{11}$.[17] Ethyl acetate was recently employed to synthesize $Li_7P_3S_{11}$ which exhibited high ionic conductivity of 1.05 mS cm^{-1} at 25 °C.[18] Among of the solvents that has been employed in $Li_7P_3S_{11}$, acetonitrile (ACN) is the most common one because the prepared SEs exhibited relatively high ionic conductivity at 25 °C, ranging from 0.8 to 1.2 mS cm^{-1}.[15,19,20] The solvent-based synthesis of $Li_7P_3S_{11}$ is complicated and could be described as dissolution-evaporation process. It was found that Li_2S reacts with P_2S_5 in ACN to form soluble $Li_4P_2S_7$ and Li_3PS_4 precipitate at a molar ratio of 1 : 1. The residue obtained after solvent removal are $Li_4P_2S_7$·ACN and Li_3PS_4·ACN. $Li_7P_3S_{11}$ was formed simultaneously with ACN removal from these phases during heat treatment at high temperature. There are many studies on how to increase the ionic conductivity of $Li_7P_3S_{11}$ produced by solid-phase reaction methods, such as using doping substances or creating defects in the crystal lattice.[21–23] However, there are still lack of the information about the method to improve the ionic conductivity of $Li_7P_3S_{11}$ prepared using liquid-phase synthesis. It was reported that CaI_2 and CaS addition enhanced the conductivity of $Li_7P_3S_{11}$.[16,24] $Li_7P_3S_{11}$ prepared

[a]*Faculty of Materials Technology, Ho Chi Minh City University of Technology (HCMUT), 268 Ly Thuong Kiet Str., Dist. 10, Ho Chi Minh City, Vietnam. E-mail: nhhphuc@hcmut.edu.vn*

[b]*Vietnam National University Ho Chi Minh City, Linh Trung Ward, Thu Duc Dist., Ho Chi Minh City, Vietnam*

[c]*VNU-HCM Key Laboratory for Material Technologies, Ho Chi Minh City University of Technology (HCMUT), 268 Ly Thuong Kiet Str., Dist. 10, Ho Chi Minh City, Vietnam*

† Electronic supplementary information (ESI) available. See DOI: https://doi.org/10.1039/d4ra00442f

using a mixture of Li_2S, P_2S_5, and excess elemental sulfur in a mixed solvent of acetonitrile, tetrahydrofuran, and ethanol also exhibited high ionic conductivity of about 1.2 mS cm^{-1} at 25 °C.[25]

In this study, the ionic conductivity of $Li_7P_3S_{11}$ prepared using ACN was enhanced by CaX_2 (X = Cl, Br, I) and LiI doping. The $95Li_7P_3S_{11}$–$5CaI_2$ solid electrolyte exhibited the ionic conductivity of about 1.0 mS cm^{-1} at 25 °C. The $90Li_7P_3S_{11}$–$5CaI_2$–5LiI solid electrolyte showed high ionic conductivity of about 3.1 mS cm^{-1} at 25 °C, which was comparable to those prepared by solid-state reaction. The data obtained from AC impedance spectroscopy was interpreted in terms of conductivity isotherms, dielectric constant and dielectric loss. It was found that CaI_2 and LiI doping enhanced the Li-ion movement at grain boundary and $P_2S_7^{4-}$ ion motion, thus improved ionic conductivity.

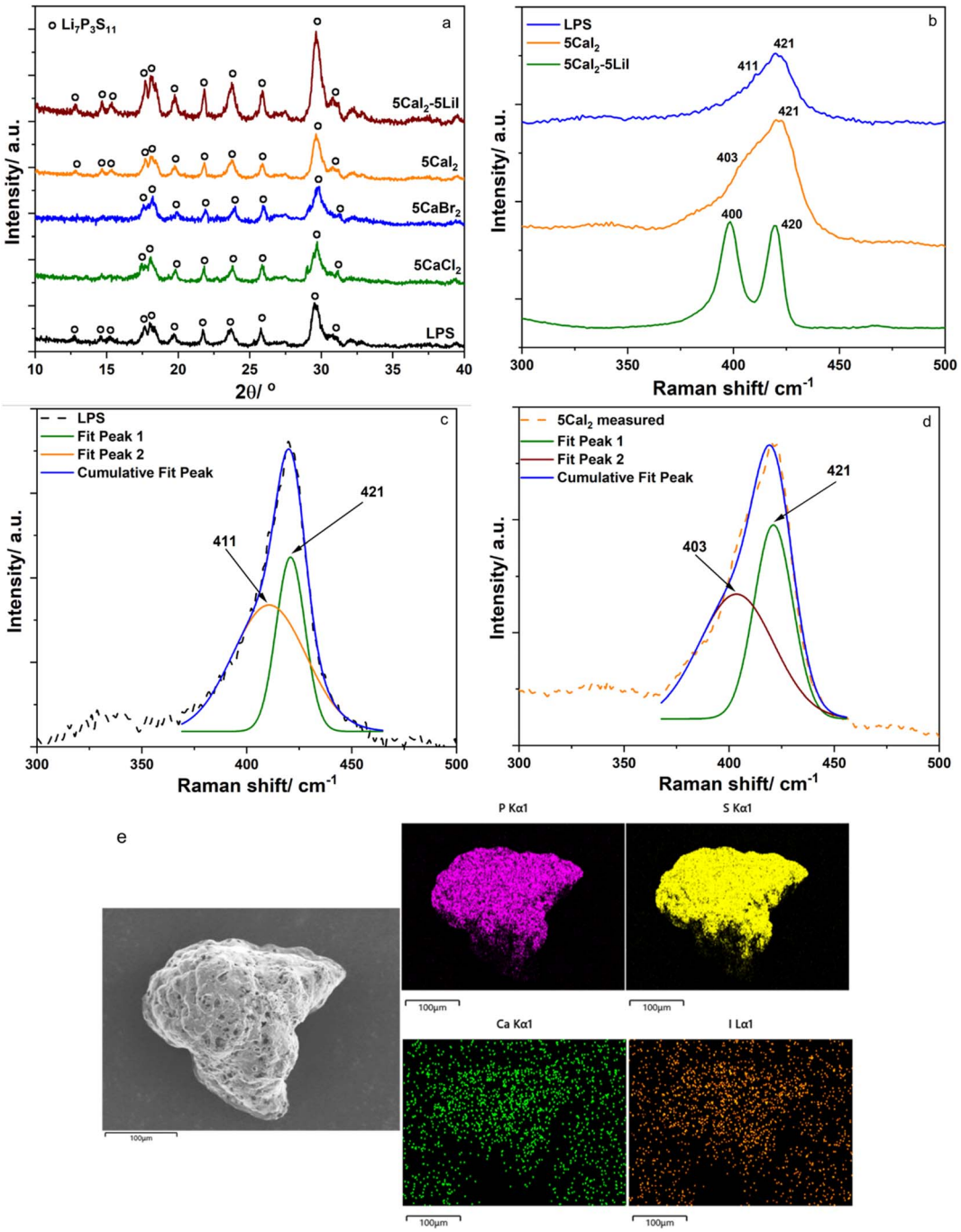

Fig. 1 Structural characterization of the prepared samples. (a) XRD patterns of $Li_7P_3S_{11}$ (LPS), $95Li_7P_3S_{11}$–$5CaX_2$ ($5CaX_2$) and $90Li_7P_3S_{11}$–$5CaI_2$–5LiI ($5CaI_2$–5LiI) solid electrolytes; (b) Raman spectra of LPS, $5CaI_2$ and $5CaI_2$–5LiI; (c and d) deconvolution of the main Raman peaks of LPS and $5CaI_2$, respectively; (e) SEM-EDS results of $5CaI_2$–5LiI.

2. Experimental

Chemicals

Li_2S (99.9%, Macklin), P_2S_5 (99%, Macklin), $CaCl_2$ (99.99%, Macklin), $CaBr_2$ (99.99%, Aladin), CaI_2 (99.999%, Macklin), LiI (99.999%, Macklin) and super dehydrated acetonitrile (Aldrich) were used as-received without any further treatment.

Liquid-phase synthesis of $Li_7P_3S_{11}$

1.5 g of Li_2S and P_2S_5 (7 : 3 in molar ratio) was weighted and put into a three-necked flask together with 40 ml of ACN. The mixture was stirred at 300 rpm and 50 °C for 24 h, the solvent was then evaporated at 80 °C under low pressure. The residue was carefully grounded using agate mortar prior to be heat treated at 270 °C for 2 h in Ar atmosphere to obtain $Li_7P_3S_{11}$ solid electrolyte (hereafter denote as LPS).

Liquid-phase synthesis of $95Li_7P_3S_{11}$–$5CaX_2$ (X = Cl, Br, I)

1.5 g of Li_2S and P_2S_5 (7 : 3 in molar ratio) and appropriate amount of CaX_2 to form $95Li_7P_3S_{11}$–$5CaX_2$ (molar ratio) was put into a three-necked flask together with 40 ml of ACN. The mixture was stirred at 300 rpm and 50 °C for 24 h, the solvent was then evaporated at 80 °C under low pressure. The residue was carefully grounded using agate mortar prior to be heat treated at 270 °C for 2 h in Ar atmosphere to obtain $95Li_7P_3S_{11}$–$5CaX_2$ solid electrolytes (hereafter denote as $5CaX_2$).

Liquid-phase synthesis of $90Li_7P_3S_{11}$–$5CaI_2$–5LiI

1.5 g of Li_2S and P_2S_5 (7 : 3 in molar ratio), appropriate amount of CaI_2 and LiI to form $90Li_7P_3S_{11}$–$5CaI_2$–5LiI (molar ratio) was put into a three-necked flask together with 40 ml of ACN. The mixture was stirred at 300 rpm and 50 °C for 24 h, the solvent was then evaporated at 80 °C under low pressure. The residue was carefully grounded using agate mortar prior to be heat treated at 270 °C for 2 h in Ar atmosphere to obtain $90Li_7P_3S_{11}$–$5CaI_2$–5LiI solid electrolyte (hereafter denote as $5CaI_2$–5LiI).

Structural characterization

The structure of the prepared samples was characterized with X-ray diffraction (XRD; X8, Bruker), Raman spectroscopy (Horiba LabRam HR spectrometer, 532 nm) and SEM (S4800, Hitachi) and EDS (ULTIM MAX, Oxford Instrument).

The samples were prepared in an Ar-filled glove box. The prepared sample was loaded into an air-tide sample holder for characterization.

AC electrochemical impedance spectroscopy

The electrical conductivity measurement was performed on a pellet prepared by uniaxially cold pressing approximately 100 mg of the powder at a pressure of 510 MPa as reported previously.[26] The alternating-current impedance spectroscopy measurement was carried out using a potentiostat (PGSTAT302N, Autolab, Herisau, Switzerland) from 10 MHz to 10 Hz. Since $5CaI_2$–5LiI exhibited high ionic conductivity at room temperature, a pellet with thickness of about 4.2 mm was prepared to get accurate data.

3. Results and discussion

Fig. 1a showed the XRD patterns of LPS, $5CaX_2$ and $5CaI_2$–5LiI solid electrolytes. The patterns of all samples could be assigned to $Li_7P_3S_{11}$ crystal phase.[7,27] No peaks of CaX_2 and LiI was detected. The position of the most intense peak in the doped samples was almost similar to that of LPS indicating that only a small amount of CaX_2 incorporated to the crystal structure of $Li_7P_3S_{11}$. It was also reported that the full doping amount of CaI_2 to $Li_7P_3S_{11}$ was about 3 mol%.[16] Ujiie *et al.* reported that LiX (X = F, Cl, Br, I) dissolved into LPS crystal structure at less than 10% molar ratio.[27] Hikima *et al.* found that CaS and CaI_2 mainly remained at the grain boundary of $Li_7P_3S_{11}$.[24] Thus, the patterns in Fig. 1a suggested that a part of CaX_2 and LiI incorporated into the structure of LPS, while the remained part existed at the grain boundary of the LPS particle. Fig. 1b showed the Raman spectra of LPS, $5CaI_2$ and $5CaI_2$–5LiI. Fig. 1c and

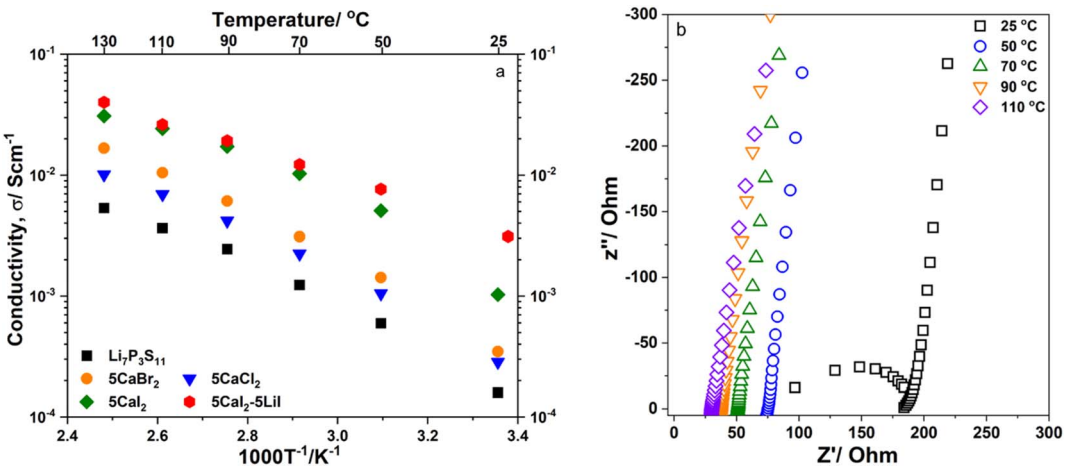

Fig. 2 (a) Temperature dependence of $Li_7P_3S_{11}$, $5CaX_2$ (X = Cl, Br, I) and $5CaI_2$–5LiI solid electrolytes; (b) electrochemical impedance spectra of the prepared $5CaI_2$–5LiI solid electrolyte.

Table 1 DC activation energy $E_{a,DC}$, activation energy $E_{a,m}$ of ion migration at grain boundary, and characteristic time $\tau_{0,m}$ of ion migration at grain boundary

	LPS	$5CaCl_2$	$5CaBr_2$	$5CaI_2$	$5CaI_2$–5LiI
$E_{a,DC}$/kJ mol^{-1}	36	37	36	30	25
$E_{a,m}$/kJ mol^{-1}	37	38	37	31	19
$\tau_{0,m}$/s	5.0×10^{-10}	3.4×10^{-10}	4.4×10^{-10}	6.3×10^{-9}	4.1×10^{-7}

d showed the deconvolution spectra of LPS and $5CaI_2$, respectively. The spectrum of LPS had two peaks at 421 and 411 cm^{-1}, which corresponded to the vibration of PS_4^{3-} and $P_2S_7^{4-}$.[28] The spectrum of $5CaI_2$ also revealed two peaks of PS_4^{3-} and $P_2S_7^{4-}$ located at 421 and 403 cm^{-1}. The spectrum of $5CaI_2$–5LiI showed two peaks located at 420 and 400 cm^{-1}, which could be assigned to the local structure unit of PS_4^{3-} and $P_2S_7^{4-}$ in $Li_7P_3S_{11}$, respectively. The peak positions of PS_4^{3-} and $P_2S_7^{4-}$ ions in samples $5CaI_2$ and $5CaI_2$–5LiI had shifted as compared to the LPS sample showing that CaI_2 addition affected the vibration of PS_4^{3-} and $P_2S_7^{4-}$ ions. The results from Raman spectra demonstrated that a portion of CaI_2 incorporated into the crystal structure of LPS. SEM-EDS results for $5CaI_2$–5LiI is shown in Fig. 1e. The SEs are in the form of particles with a size of several tens of micrometers. EDS results indicated that CaI_2 and LiI were well dispersed in the prepared powder sample. It can be reasonably concluded that Ca^{2+} and I^- were doped in the $Li_7P_3S_{11}$ structure based on the experimental results: the disappearance of the peak corresponding to CaI_2 and LiI in the XRD results, the peak shift in the Raman spectrum, Ca and I are also dispersed in the particles as shown in the EDS results.

The temperature dependence of the ionic conductivity of LPS, $5CaX_2$ and $5CaI_2$–5LiI solid electrolytes were illustrated in Fig. 2a. The electrochemical impedance spectra of $5CaI_2$–5LiI, which were employed to calculate ionic conductivity, were illustrated in Fig. 2b. Those of LPS and $5CaI_2$ were shown in Fig. S1 (ESI).† The ionic conductivity at 25 °C of LPS, $5CaCl_2$, $5CaCl_2$, $5CaCl_2$ and $5CaI_2$–5LiI were 0.15, 0.19, 0.25, 1.0 and 3.1 mS, respectively. At 70 °C, the ionic conductivity of all the samples increased and reached the value of 1.05, 2.0, 2.2, 10.1 and 13 mS for LPS, $5CaCl_2$, $5CaCl_2$, $5CaCl_2$ and $5CaI_2$–5LiI, respectively. It could be seen that $\log_{10}(\sigma)$ satisfied an almost linear dependence on inversed temperature and therefore followed Arrhenius equation $\sigma = \sigma_0 \exp(-E_{a,DC}/(k_B T))$. The

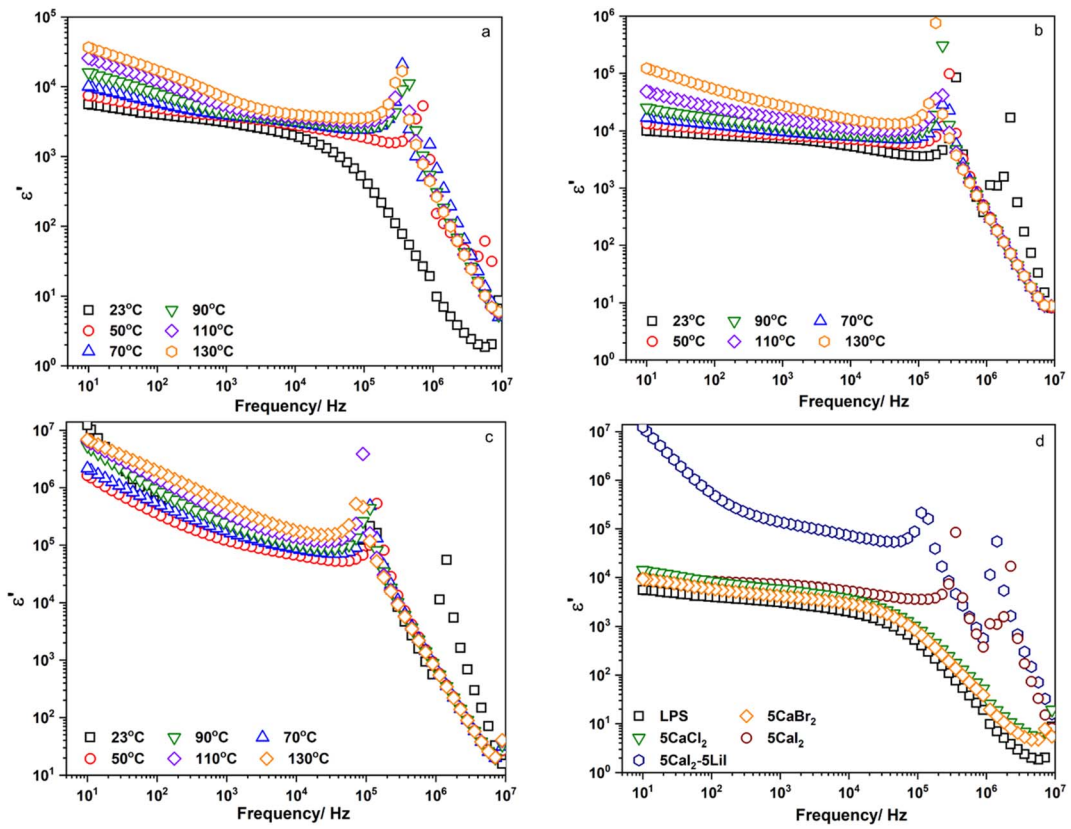

Fig. 3 Frequency dependence of the real part of dielectric constant, ε', of (a) LPS, (b) $5CaI_2$, (c) $5CaI_2$–5LiI measured at different temperature and (d) frequency dependence of ε' of LPS, $5CaCl_2$, $5CaBr_2$, $5CaI_2$, $5CaI_2$–5LiI measured at room temperature.

activation energy $E_{a,DC}$ was then calculated and shown in Table 1. The activation energy $E_{a,DC}$ of LPS, $5CaCl_2$, $5CaCl_2$, $5CaCl_2$ and $5CaI_2$–5LiI were 36, 37, 36, 30 and 25 kJ mol^{-1}, respectively. The results showed that CaI_2 and LiI addition greatly improved the ionic conductivity and activation energy of LPS.

The study of dielectric properties provides information on electrical energy decay in materials with alternating electric fields. The real part of the dielectric constant, ε', reflects the amount of energy stored in the form of polarization when an electric field is applied.[29] The real part of the permittivity, ε', was calculated using the following equation:

$$\varepsilon' = -\frac{Z''}{\omega C_0\left(Z'^2 + Z''^2\right)}$$

where $C_0 = \varepsilon_0(A/d)$ is the free space capacitance of the cell, ε_0 is the permittivity of the free space (8.854×10^{-12} F m^{-1}), and A and d are the surface area and thickness, respectively, of the sample pellet.

Fig. 3 showed the frequency dependence of the real part of dielectric constant, ε', of (a) LPS, (b) $5CaI_2$, (c) $5CaI_2$–5LiI measured at different temperature and (d) frequency dependence of ε' of LPS, $5CaCl_2$, $5CaBr_2$, $5CaI_2$, $5CaI_2$–5LiI measured at room temperature. The observed upturn in all plots at lower frequencies could be attributed to the electrode–electrolyte interface polarization. This is because the accumulation of charged ions near the electrode leads to the formation of space charge layer, which in turn block the electric field and enhance electrical polarization. As frequency increased, the dielectric constant decreased. This phenomenon is a typical property of ionic conducting materials.[30] An increase in ε' with an increase in temperature was observed at low and intermediate frequency region in all the samples suggesting that charge carrier movement at grain boundary was thermally activated (Fig. 3 and S2†). The plots of LPS, $5CaCl_2$ and $5CaBr_2$ at room temperature continuously decreased in intermediate and high frequency region; however, the plots of $5CaI_2$ and $5CaI_2$–5LiI at room temperature exhibited a maxima at 10^5–10^6 Hz (Fig. 3d). The maxima were observed at 10^5–10^6 Hz in all the plots at 50 °C or above (Fig. 3 and S1†). Those observation suggested that CaI_2 and LiI addition enhanced dielectric properties of $Li_7P_3S_{11}$. This observation was in agreement with Raman spectra (Fig. 1b) and ionic conductivity at room temperature of the prepared samples (Fig. 2).

Fig. 4a–c showed the frequency dependence of the loss factor, tan δ, of LPS, $5CaI_2$ and $5CaI_2$–5LiI, respectively. The plot at room temperature of LPS showed two peaks at low and high frequency, which could be attributed to ion migration at grain boundary and bulk (Fig. 4a). As temperature increased, two peaks appeared at low frequency region. The one at lower frequency was assigned to electrode polarization. The peak at

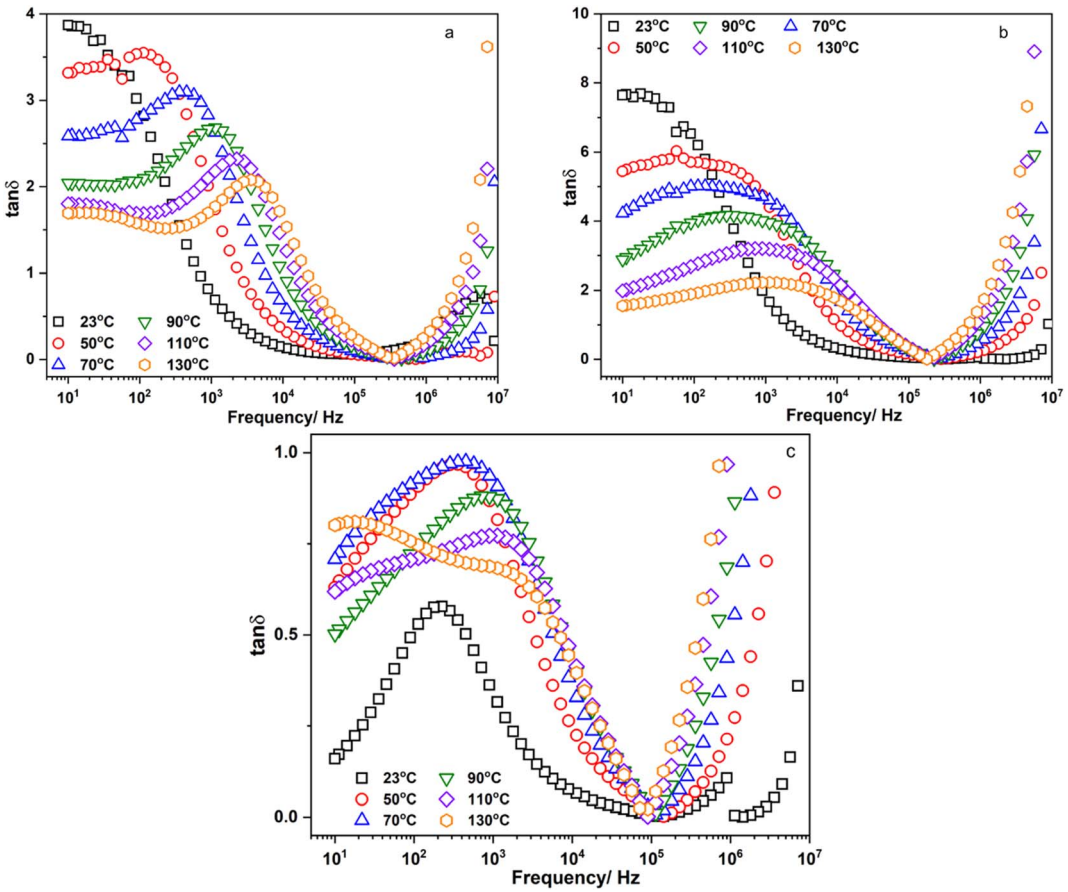

Fig. 4 Frequency dependence of the loss factor, tan δ, of (a) LPS, (b) $5CaI_2$ and (c) $5CaI_2$–5LiI.

higher frequency shifted toward high frequency as temperature increased and could be attributed to grain boundary migration. The migration energy $E_{a,m}$ of the Li^+ ion moving at grain boundary could be obtained from the temperature dependence of the peak position at low frequency in tan δ. Temperature dependence of the inverse relaxation time ($\tau_m^{-1} = F_{max}$) was plotted, and the migration characteristic time $\tau_{0,m}$ was then obtained by numerically fitting the data using the Arrhenius equation: $\tau_m = \tau_{0,m} \exp(-E_{a,m}/(k_B T))$. The obtained $E_{a,m}$ and $\tau_{0,m}$ were illustrated in Table 1. The migration activation energy at grain boundary $E_{a,m}$ of the prepared samples were similar to DC activation energy $E_{a,DC}$, suggesting that charge carrier moving at grain boundary was the critical process in those samples. The characteristic migration time of LPS, $5CaCl_2$ and $5CaBr_2$ were 5.0×10^{-10}, 3.4×10^{-10} and 4.4×10^{-10} s, respectively. The characteristic migration time of $5CaI_2$ and $5CaI_2$–5LiI were 6.3×10^{-9} and 4.1×10^{-7} s, respectively. Therefore, the charge carrier movement at grain boundary was enhanced by CaI_2 and LiI addition; it changed from short range diffusion in LPS to long range diffusion in $5CaI_2$ and $5CaI_2$–5LiI. This phenomenon was also consistent with the article by Tu *et al.*, which reported the influence of LiI doping on the impedance at the grain boundary of Li_2S–AlI_3 solid solution.[31]

4. Conclusion

$Li_7P_3S_{11}$ solid electrolytes doped with CaX_2 (X = Cl, Br, I) and LiI were successfully prepared by liquid-phase synthesis using ACN as reaction medium. Results from XRD, Raman spectroscopy and SEM-EDS proved that CaX_2 and LiI incorporated into the crystal structure of $Li_7P_3S_{11}$. Results from AC electrochemical impedance spectroscopy showed that CaI_2 and LiI addition enhanced dielectric properties of $Li_7P_3S_{11}$. In addition, the charge carrier movement at grain boundary changed from short range diffusion in LPS to long range diffusion in $5CaI_2$ and $5CaI_2$–5LiI. As a result, very high ionic conductivity of 3.1 mS cm^{-1} at 25 °C was obtained.

Conflicts of interest

The authors declare that they have no known competing financial interests or personal relationships that could have appeared to influence the work reported in this paper.

Acknowledgements

We acknowledge Ho Chi Minh City University of Technology (HCMUT), VNU-HCM for supporting this study.

References

1 S. Chen, D. Xie, G. Liu, J. P. Mwizerwa, Q. Zhang, Y. Zhao, X. Xu and X. Yao, Sulfide solid electrolytes for all-solid-state lithium batteries: structure, conductivity, stability and application, *Energy Storage Mater.*, 2018, **14**, 58–74.

2 J. Lau, R. H. DeBlock, D. M. Butts, D. S. Ashby, C. S. Choi and B. S. Dunn, Sulfide Solid Electrolytes for Lithium Battery Applications, *Adv. Energy Mater.*, 2018, **8**, 201800933.

3 Y. Seino, T. Ota, K. Takada, A. Hayashi and M. Tatsumisago, A sulphide lithium super ion conductor is superior to liquid ion conductors for use in rechargeable batteries, *Energy Environ. Sci.*, 2014, **7**, 627–631.

4 Y. Kato, S. Hori, T. Saito, K. Suzuki, M. Hirayama, A. Mitsui, M. Yonemura, H. Iba and R. Kanno, High-power all-solid-state batteries using sulfide superionic conductors, *Nat. Energy*, 2016, **1**, 16030.

5 P. Adeli, J. D. Bazak, A. Huq, G. R. Goward and L. F. Nazar, Influence of Aliovalent Cation Substitution and Mechanical Compression on Li-Ion Conductivity and Diffusivity in Argyrodite Solid Electrolytes, *Chem. Mater.*, 2020, **33**, 146–157.

6 Y. Subramanian, R. Rajagopal and K.-S. Ryu, Synthesis of Sb-doped $Li_{10}P_3S_{12}I$ solid electrolyte and their electrochemical performance in solid-state batteries, *J. Energy Storage*, 2024, **78**, 109943.

7 F. Mizuno, A. Hayashi, K. Tadanaga and M. Tatsumisago, New, Highly Ion-Conductive Crystals Precipitated from Li_2S–P_2S_5 Glasses, *Adv. Mater.*, 2005, **17**, 918–921.

8 M. K. Tufail, N. Ahmad, L. Yang, L. Zhou, M. A. Naseer, R. Chen and W. Yang, A panoramic view of $Li_7P_3S_{11}$ solid electrolytes synthesis, structural aspects and practical challenges for all-solid-state lithium batteries, *Chin. J. Chem. Eng.*, 2021, **39**, 16–36.

9 B. Huang, X. Yao, Z. Huang, Y. Guan, Y. Jin and X. Xu, Li_3PO_4-doped $Li_7P_3S_{11}$ glass-ceramic electrolytes with enhanced lithium ion conductivities and application in all-solid-state batteries, *J. Power Sources*, 2015, **284**, 206–211.

10 M. Eom, S. Choi, S. Son, L. Choi, C. Park and D. Shin, Enhancement of lithium ion conductivity by doping Li_3BO_3 in Li_2S-P_2S_5 glass-ceramics electrolytes for all-solid-state batteries, *J. Power Sources*, 2016, **331**, 26–31.

11 P. Lu, F. Ding, Z. Xu, J. Liu, X. Liu and Q. Xu, Study on (100-x)($70Li_2S$-$30P_2S_5$)-xLi_2ZrO_3 glass-ceramic electrolyte for all-solid-state lithium-ion batteries, *J. Power Sources*, 2017, **356**, 163–171.

12 Y. Guo, H. Guan, W. Peng, X. Li, Y. Ma, D. Song, H. Zhang, C. Li and L. Zhang, Enhancing the electrochemical performances of Li_7P3S_{11} electrolyte through P_2O_5 substitution for all-solid-state lithium battery, *Solid State Ionics*, 2020, **358**, 115506.

13 M. Murakami, K. Shimoda, S. Shiotani, A. Mitsui, K. Ohara, Y. Onodera, H. Arai, Y. Uchimoto and Z. Ogumi, Dynamical Origin of Ionic Conductivity for $Li_7P_3S_{11}$ Metastable Crystal As Studied by $^{6/7}$Li and ^{31}P Solid-State NMR, *J. Phys. Chem. C*, 2015, **119**, 24248–24254.

14 Y. Seino, M. Nakagawa, M. Senga, H. Higuchi, K. Takada and T. Sasaki, Analysis of the structure and degree of crystallisation of $70Li_2S$–$30P_2S_5$ glass ceramic, *J. Mater. Chem. A*, 2015, **3**, 2756–2761.

15 M. Calpa, N. C. Rosero-Navarro, A. Miura and K. Tadanaga, Electrochemical performance of bulk-type all-solid-state batteries using small-sized $Li_7P_3S_{11}$ solid electrolyte

prepared by liquid phase as the ionic conductor in the composite cathode, *Electrochim. Acta*, 2019, **296**, 473–480.

16 N. H. H. Phuc, H. Gamo, K. Hikima, H. Muto and A. Matsuda, Preparation of CaI_2-Doped $Li_7P_3S_{11}$ by Liquid-Phase Synthesis and Its Application in an All-Solid-State Battery with a Graphite Anode, *Energy Fuels*, 2022, **36**, 4577–4584.

17 S. Ito, M. Nakakita, Y. Aihara, T. Uehara and N. Machida, A synthesis of crystalline $Li_7P_3S_{11}$ solid electrolyte from 1,2-dimethoxyethane solvent, *J. Power Sources*, 2014, **271**, 342–345.

18 J. Zhou, Y. Chen, Z. Yu, M. Bowden, Q. R. S. Miller, P. Chen, H. T. Schaef, K. T. Mueller, D. Lu, J. Xiao, J. Liu, W. Wang and X. Zhang, Wet-chemical synthesis of $Li_7P_3S_{11}$ with tailored particle size for solid state electrolytes, *Chem. Eng. J.*, 2022, **429**, 132334.

19 R. C. Xu, X. H. Xia, Z. J. Yao, X. L. Wang, C. D. Gu and J. P. Tu, Preparation of $Li_7P_3S_{11}$ glass-ceramic electrolyte by dissolution-evaporation method for all-solid-state lithium ion batteries, *Electrochim. Acta*, 2016, **219**, 235–240.

20 M. Calpa, N. C. Rosero-Navarro, A. Miura and K. Tadanaga, Preparation of sulfide solid electrolytes in the Li_2S–P_2S_5 system by a liquid phase process, *Inorg. Chem. Front.*, 2018, **5**, 501–508.

21 L. Zhou, M. K. Tufail, N. Ahmad, T. Song, R. Chen and W. Yang, Strong Interfacial Adhesion between the Li_2S Cathode and a Functional $Li_7P_{2.9}Ce_{0.2}S_{10.9}Cl_{0.3}$ Solid-State Electrolyte Endowed Long-Term Cycle Stability to All-Solid-State Lithium-Sulfur Batteries, *ACS Appl. Mater. Interfaces*, 2021, **13**, 28270–28280.

22 A. Hayashi, K. Minami, S. Ujiie and M. Tatsumisago, Preparation and ionic conductivity of $Li_7P_3S_{11-z}$ glass-ceramic electrolytes, *J. Non-Cryst. Solids*, 2010, **356**, 2670–2673.

23 K. Minami, A. Hayashi, S. Ujiie and M. Tatsumisago, Electrical and electrochemical properties of glass–ceramic electrolytes in the systems Li_2S–P_2S_5–P_2S_3 and Li_2S–P_2S_5–P_2O_5, *Solid State Ionics*, 2011, **192**, 122–125.

24 K. Hikima, I. Kusaba, H. Gamo, N. H. H. Phuc, H. Muto and A. Matsuda, High Ionic Conductivity with Improved Lithium Stability of CaS- and CaI_2-Doped $Li_7P_3S_{11}$ Solid Electrolytes Synthesized by Liquid-Phase Synthesis, *ACS Omega*, 2022, **7**, 16561–16567.

25 H. Gamo, J. Nishida, A. Nagai, K. Hikima and A. Matsuda, Solution Processing via Dynamic Sulfide Radical Anions for Sulfide Solid Electrolytes, *Adv. Energy Sustainability Res.*, 2022, **3**, 2200019.

26 M. Atsunori, G. Hirotada and N. H. H. Phuc, Preparation of cubic Na_3PS_4 by liquid-phase shaking in methyl acetate medium, *Heliyon*, 2019, **5**, e02760.

27 S. Ujiie, T. Inagaki, A. Hayashi and M. Tatsumisago, Conductivity of $70Li_2S \cdot 30P_2S_5$ glasses and glass–ceramics added with lithium halides, *Solid State Ionics*, 2014, **263**, 57–61.

28 B. Zhao, J. Wu, Z. Wang, W. Ma, Y. Shi, Y. Jiang, J. Jiang, X. Liu, Y. Xu and J. Zhang, Incorporation of lithium halogen in $Li_7P_3S_{11}$ glass-ceramic and the interface improvement mechanism, *Electrochim. Acta*, 2021, **390**, 138849.

29 D. M. A. Basset, S. Mulmi, M. S. El-Bana, S. S. Fouad and V. Thangadurai, Synthesis and characterization of novel Li-stuffed garnet-like $Li_{5+2x}La_3Ta_{2-x}Gd_xO_{12}$ ($0 </= x </= 0.55$): structure-property relationships, *Dalton Trans.*, 2017, **46**, 933–946.

30 A. Molak, M. Paluch, S. Pawlus, J. Klimontko, Z. Ujma and I. Gruszka, Electric modulus approach to the analysis of electric relaxation in highly conducting $(Na_{0.75}Bi_{0.25})(Mn_{0.25}Nb_{0.75})O_3$ceramics, *J. Phys. D: Appl. Phys.*, 2005, **38**, 1450–1460.

31 T. A. Tu, N. H. H. Phuc, L. T. Q. Anh and T. V. Toan, Preparation of Li_2S-AlI_3-LiI Composite Solid Electrolyte and Its Application in All-Solid-State Li-S Battery, *Batteries*, 2023, **9**, 290–300.